A Consistent Measurement-Based Picture of Core-Mix in Direct-Drive Implosions on OMEGA

Introduction

The central goal of direct-drive implosions on the OMEGA laser[1] is to validate the performance of the high-gain, direct-drive ignition designs[2] planned for use on the National Ignition Facility. Inferring the density, temperature, and fuel–shell mix of ignition-relevant capsule implosions is important in validating models of implosions. To this end, diagnostic information from sets of implosions that differ in their hydrodynamic properties has been obtained in direct-drive spherical-capsule implosions on OMEGA. In this article, we report on an analysis of the experimental charged-particle and neutron data that provide consistent information on densities and temperatures of one set of similar experiments.

In direct-drive implosions, a spherical target is illuminated uniformly with a laser. Any degradation in target performance is believed to occur primarily through the Rayleigh–Taylor instability,[3] which is seeded by either target imperfections or laser nonuniformity. This instability, occurring at the ablation surface during the acceleration phase of the implosion, can then feed through to the fuel–shell interface and add to any pre-existing roughness on the inner surface. During the deceleration phase, these distortions at the fuel–shell interface grow, resulting in a mixing of the fuel and shell material. Neutron and charged-particle diagnostics carry direct information about this phase of the implosion, when fuel densities and temperatures are high enough for their production.

Several complementary approaches can be used to analyze the implosion observables. One route is to infer, from individual diagnostics, parameters such as the fuel areal density, which is a measure of compression. Comparisons of inferred quantities with those from simulations indicate the closeness of the actual implosions to the simulations. The problem with this technique is usually that simple models used to infer key quantities from individual diagnostics (such as "ice-block" models) may not apply to the actual implosion. Further, this technique ignores complementary information from other diagnostics that may be critical to devising the correct model. Another possible technique is to directly simulate the experiment and post-process the simulation for the relevant diagnostic. Again, the comparison is very model dependent, and further light on any disagreement between simulations and experiment is difficult to obtain through this route. The third method, described in this article, is to use all observables from a set of hydrodynamically similar implosions and infer a picture that is consistent across all diagnostics. This picture would correspond to a neutron-weighted, "1-D" description of temperature and density profiles in the core and mix region of the imploding target. The advantage of such a scheme is that it provides a picture using all available information and allows for more detailed comparisons between simulation and experiment through a sensitivity analysis of the model parameters.

In this article, we describe a consistent picture, inferred from different diagnostics, of conditions in the fuel core and mix region for 20-μm-thick-plastic-shell implosions. These targets are of interest because their stability during the acceleration phase is calculated to be similar to those predicted for OMEGA cryogenic implosions,[4] which, in turn, are energy-scaled surrogates[5] for direct-drive ignition targets.[2] Studies on these targets should then be applicable to both OMEGA cryogenic and NIF ignition targets. Experiments with plastic targets also offer a larger array of diagnostic techniques, allowing for more information on target behavior.

The following sections (1) describe the targets modeled and the diagnostics used to probe these targets, (2) present evidence for mixing and the mix model, and (3) present our conclusions.

Targets and Diagnostics

The experiments chosen for this analysis had nominally identical laser pulse shapes, smoothing conditions, target-shell thickness, and gas pressure. The makeup of the fill gas or details of the shell layers were then varied so that complementary diagnostics could be applied to hydrodynamically similar implosions. Since implosions on OMEGA show excellent reproducibility,[4] variation between different shots is relatively small, allowing for such an analysis. We consider targets with 20-μm-thick plastic shells (pure CH or with CD layers) with

different gas fills (D_2, DT, ^{3}He) at 15 atm (see Fig. 86.29 for a description of targets and corresponding observables). These targets were irradiated with a 1-ns square laser pulse with 23-kJ energy and used full-beam smoothing (2-D smoothing by spectral dispersion with 1-THz bandwidth and polarization smoothing using birefringent wedges).

For the D_2-filled targets, the neutron diagnostics involved measurements of primary neutron yields from the DD reactions and neutron-averaged ion temperatures, measured using neutron time-of-flight detectors.[4] In addition, secondary neutron yields,[6] which are produced by the following sequence of reactions,

$$D + D \rightarrow T + p$$

$$T + D \rightarrow \alpha + n(12 \sim 17 \text{ MeV}), \tag{1}$$
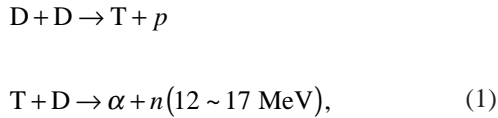
are also measured using current-mode detectors.[7] Tritons in the primary DD reaction produced at energies of about 1 MeV cause secondary reactions with the fuel deuterons as they move through the target. The ratio of the secondary neutron yields to the primary DD neutron yields depends on the fuel areal

(a)

CH
DD or DT

Primary neutrons
Secondary neutrons: $T, \rho R_f$
$<T>$ion
Secondary protons: $T, \rho R_f$
Elastically scattered
    deuterons and tritons (DT): ρR_f
Neutron-production rates

(b)

CH
CD
DD or ^{3}He

Primary neutrons
Secondary neutrons
Secondary protons
$<T>$ion
Neutron-production rates
Primary D^{3}He protons
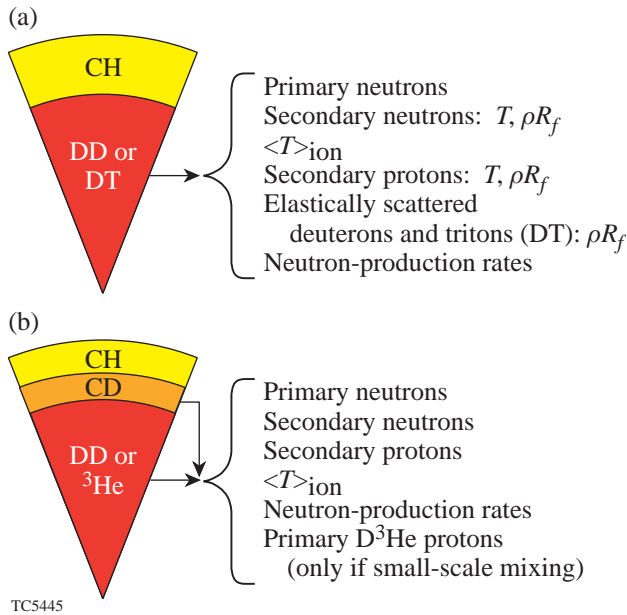   (only if small-scale mixing)

TC5445

Figure 86.29
A large suite of diagnostics has been brought to bear on plastic shells with and without CD layers and with different gas fills. The different targets and the observables that are characteristic of the targets are shown.

density. Secondary neutron yields can also depend sensitively, however, on the temperatures in the target, through the slowing down of the triton and the energy-dependent cross section of the reaction. With the cross section increasing significantly with decreasing energy of the triton (the cross section increases by nearly a factor of 5 between the triton birth energy and about 0.1 MeV), this diagnostic is particularly sensitive to the effects of mix; the shell material mixed in with the fuel could contribute to the greater slowing down of the triton and consequently an increased secondary neutron yield.

Secondary protons,[8] in an analogous reaction to that of the secondary neutrons, are produced in D_2-filled targets. Here, the second main branch of the DD reaction produces primary ^{3}He particles, which in turn fuse with the background deuterons as they traverse the fuel region:

$$D + D \rightarrow {}^3\text{He} + n$$

$${}^3\text{He} + D \rightarrow \alpha + p(12 \sim 17 \text{ MeV}). \tag{2}$$
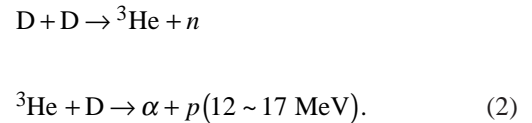
Again, this reaction is dependent on the areal density of the fuel and the slowing down of the primary ^{3}He particles. In this case, however, the cross section of the reaction decreases significantly with increasing slowing down of the ^{3}He particle. Therefore, when slowing down is significant, the areal density local to the primary ^{3}He production essentially determines the secondary proton yield. Measurements of secondary proton spectra are carried out using a magnet-based charged-particle spectrometer (CPS) as well as "wedge-range-filter"-based spectrometers using CR-39 track detectors.[8]

The number of elastically scattered deuterons and tritons ("knock-ons") is directly proportional to the fuel areal density for DT-filled targets.[9] Since the elastic scattering of the 14-MeV DT neutrons off the background fuel ions produces these particles, these diagnostics are relatively insensitive to the location of the fuel and therefore mix. A forward-scattered peak in the particle spectrum characterizes this diagnostic. The number of knock-on particles in this forward-scattered peak is expected to be a constant fraction of the total produced and therefore provides a measure of the total fuel areal density. Detailed knock-on particle spectra have been measured using the CPS and used to infer areal density in DT-filled targets.[10]

In addition to the plastic shells mentioned above, direct information regarding the clean core of fuel and the mixing of the fuel and shell can be obtained from plastic-shell implosions

with an embedded CD layer and with ^{3}He fill [Fig. 86.29(b)]. With a CD layer an observable signal of primary D^{3}He protons is produced when a significant number of deuterons from the CD layer come into contact with the ^{3}He in the fuel. Again, the proton yield is measured using the CPS. Preliminary experiments have used targets with the CD layer at both the fuel–shell interface and a distance of 1 μm displaced from this interface.

Evidence of Mixing and the Mix Model

A comparison of particle yields with those from 1-D simulations using *LILAC*[11] suggests mixing of the fuel and shell. Figure 86.30 shows experimental observables and results from the corresponding 1-D simulations that contain no effects of mixing. The relatively model independent knock-ons indicate fuel areal densities of 15 mg/cm^2, nearly 93% of 1-D values. Figure 86.30 also indicates, however, that the neutron yields from the DD reaction are only about 33% of 1-D. One explanation for this reduction in the yield is the mixing of cold shell material into the hot fuel. The fuel consequently cools, quenching the yield. In the unmixed 1-D simulations, most of the neutron yield is produced at a radius that is about two-thirds the distance from the fuel–shell interface. Therefore, a small amount of mixing can considerably lower temperatures in this region and consequently quench the yield. Secondary neutron ratios that are higher in the experiment than in the simulations can also be explained using the same mixing scenario. In this case, the lower temperatures result in a larger slowing down of the intermediate tritons, and the resultant higher cross section

enhances the secondary neutron yield relative to unmixed 1-D simulations. Finally, direct evidence from experiment for small-scale mixing has been obtained from plastic shells with a 1-μm CD layer at the fuel–shell interface. With a ^{3}He fill, proton yields from the D^{3}He reaction are produced only if the ^{3}He is mixed with the deuterium from the CD layer. *LILAC* simulations with a ^{3}He gas fill, in principle, give zero yields for these protons. A conservative estimate of the proton yield can be obtained by assuming that the ^{3}He gas is isobarically diffused throughout the shell. The measured yields are nearly 50,000% higher than the simulation values, indicating the occurrence of small-scale mix.

The model used to describe the results presented above assumes a clean fuel region and a mixed region consisting of both fuel and shell material (Fig. 86.31). The mass of the fuel is fixed and corresponds to that of 15 atm of gas fill. Density and temperature are assumed to be constant in the clean fuel region and vary linearly in the mixed region. Further, the temperatures of the electrons and ions are assumed to be the same. This approximation can be justified since the equilibration time for electron and ion temperatures at these conditions is typically less than 5 ps. The model (Fig. 86.31) is described by six parameters (five free parameters since the mass of the fuel is known): the radius of the clean fuel region, the density of the clean region, the radius of the mixed region, the density of the shell material at the outer edge of the mix region, the temperature of the fuel in the clean region, and the temperature

(a)

	Experiment (average over four shots)	Experiment (% of 1-D *LILAC*)
Fuel ρR (DT)	15±2	9
Neutron yield	$(1.6\pm0.05) \cdot 10^{11}$	33
Secondary-neutron ratio	$(2.4\pm0.4) \cdot 10^{-3}$	139

(b)

D^{3}He proton yield	$4 \cdot 10^7$	~10,000*

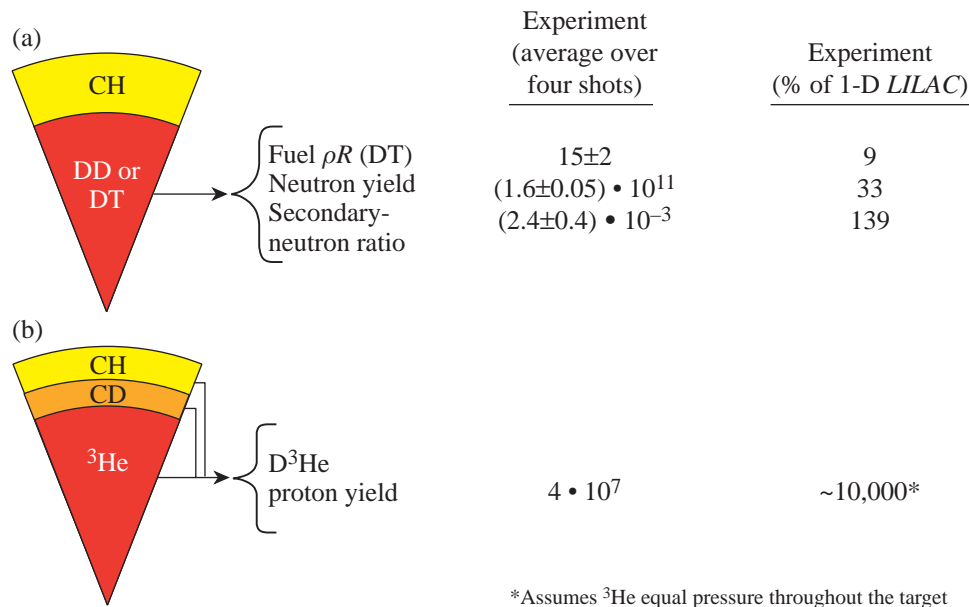*Assumes ^{3}He equal pressure throughout the target

TC5446

Figure 86.30

Evidence for mixing: primary yields and secondary ratios suggest mixing of the fuel and the shell. Despite a smaller inferred fuel areal density in the experiment, the secondary neutron yield ratio is higher than in 1-D simulations. Direct evidence for mixing comes from the enhanced D^{3}He proton yield relative to 1-D simulations for the ^{3}He-filled targets.

of the shell material at the outer edge of the mixed region. Operationally, using the mass and a guess for the total and clean fuel areal density, one uniquely solves for the two radii and fuel density. A guess for the shell mass in the mixed region is made, which uniquely determines the shell-density profile. The guesses for the two fuel areal densities, the shell mass, and the temperatures are varied, and for each static model the yields for the secondary neutron and proton reactions, the neutron-production rates, and the neutron-averaged ion temperatures are calculated. This is repeated until good agreement with experimental data is obtained. The yields from the ^{3}He-filled targets are calculated using the optimal profiles and by replacing the DD or DT fuel with ^{3}He.

Particle yields are calculated using the Monte Carlo particle-tracking code *IRIS*. *IRIS* tracks particles in straight-line trajectories on a spherically symmetric mesh. Products of primary reactions are launched based on the location of the fuel and temperature and density distributions in the target. Secondary reactions are produced along primary trajectories, and secondary trajectories in turn are launched according to the differential cross section of the reaction. The energy loss of charged particles is continuous; the trajectory is divided into smaller sections, and at the end of each section the energy of the particle is updated, accounting for its energy loss over that

section. *IRIS* runs in the so-called "embarrassingly parallel" mode on an SGI Origin 2000 machine using MPI.[12] In this mode an identical copy of *IRIS* is placed on each processor, and, at the end of the simulation, yields and spectra are tallied.

The optimal profiles from this parameter variation are shown in Fig. 86.31. The profiles from the corresponding *LILAC* simulation at peak particle production are also overlaid on the figure. The narrow ranges on the figure indicate the tight constraints on the model parameters. For this set of parameters, which reproduces experimental data, the fuel areal density is distributed approximately equally between the clean and mixed regions. The shell mass in the mixing region [Fig. 86.31(a)] corresponds to a 0.5- to 1-μm-thick layer of the initial shell material mixing into the fuel region; the optimum fit occurs with about 1 μm of mixing. This shell areal density in the mixed region is about 20% of the compressed shell areal density inferred from other diagnostics such as the energy loss of the D^{3}He proton from the D^{3}He-filled targets.[4] The density and temperature profiles compare very well with those from simulation, suggesting that these implosions are nearly 1-D in their compression; a small amount of mixing redistributes material near the fuel–shell interface without significantly altering the hydrodynamics of the implosion.
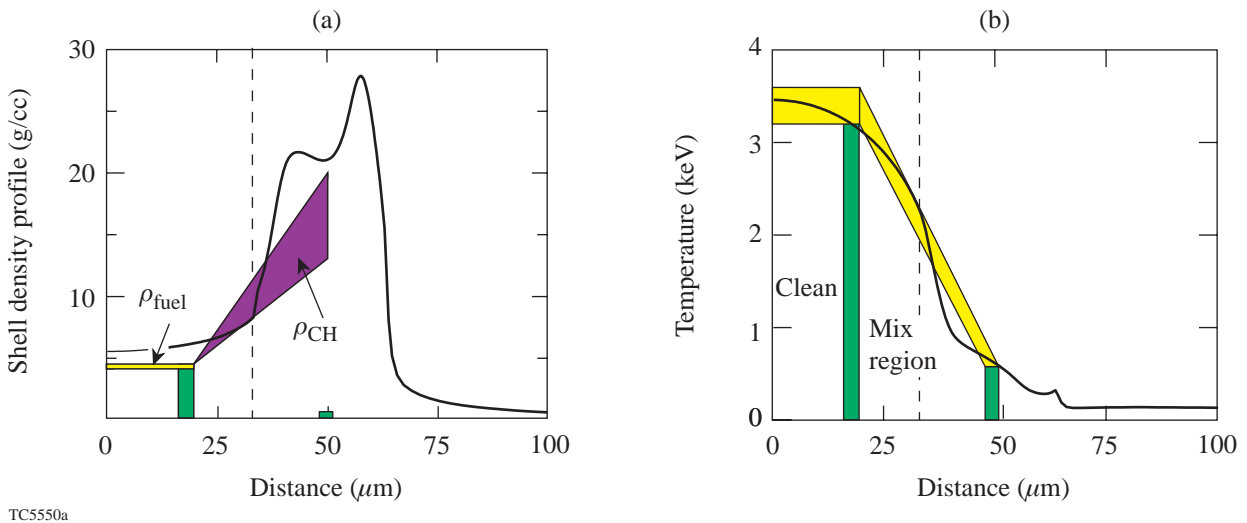
TC5550a

Figure 86.31
Core and fuel–shell mix density (a) and temperature (b) profiles inferred from the mix model. The range of the parameters, which is consistent with experimental observables, is shown by the width of the various parameter bands. The fuel–shell interface predicted by *LILAC* is shown as a dotted line in both. The dark solid lines represent the *LILAC*-predicted density and temperature profiles at peak neutron production.

The yields from the optimal profile are compared to experimental observables in Table 86.II. The model reproduces the experimental fuel areal densities, secondary neutron, proton ratio, and the neutron-averaged ion temperature. The time-dependent burn rate is also measured using the neutron temporal diagnostic (NTD)[13] in the experiment. The burn rate in this static model is less than the maximum measured burn rate. A burn width for DD-filled targets can be calculated using the experimental DD yield and the burn rate in the static model for different fills. For instance, for the ^{3}He fill in CD layer targets, this calculated burn width from DD targets is used to obtain yields from the static model. These yields are also in good agreement with the data.

Further evidence supporting this model has been obtained from recent implosion experiments on a 20-μm CH shell with a ^{3}He gas fill and with a 1-μm CD layer offset from the fuel–shell interface by 1 μm. The D^{3}He proton yields measured from this implosion are reduced significantly relative to the zero-offset CD layer implosion (preliminary proton yield ~7×10^5 compared to 1×10^7 for the zero-offset case). The significantly lower number suggests that more than 90% of the mix-related yield is due to approximately 1 μm of the initial shell mixing into the fuel.

Pre-existing modes at the inner surface of the plastic shell and/or feedthrough of these modes have been considered earlier as possible sources of nonuniformities during the deceleration phase of ICF implosions.[14] Multidimensional simulations, currently being pursued, are necessary to determine if feedthrough of the higher-order modes is significant for implosions on OMEGA and if the subsequent RT growth can account for the relatively small scales inferred from the experiments.

Conclusions

A large set of direct-drive implosions on OMEGA has been devoted to imploding hydrodynamically similar implosions with different gas fills and shell compositions. A complementary set of diagnostics has been obtained from such implosions, allowing for a more detailed analysis of the core and mix region of these targets. A static picture of 20-μm-thick-shell, direct-drive implosions on OMEGA has been presented. This model assumes a clean fuel region and a "mix" region where the shell material is mixed into the fuel. Excellent agreement with the suite of neutron and particle diagnostics is obtained through such a model. The model suggests that about 1 μm of the initial shell material is mixed into the fuel during nuclear-particle production and is responsible for the observed yield ratios. The model also suggests that the fuel areal density is distributed

Table 86.II: The model reproduces many experimental observables with 1 μm of shell material mixed into the fuel.

Fill	Shell	Parameter	Measurement	Model (% of expt)
DT	CH	Fuel ρR (mg/cm^2) (DT fill)	15±2	100
		T_{ion} (DT) (keV)	4.4±0.4±0.5 (sys)	86
D$_2$	CH	Max: neutron burn rate (n/s)	$(9\pm1) \times 10^{20}$	110
		T_{ion} (D$_2$) (keV)	3.7±0.2±0.5 (sys)	89
		Secondary neutron ratio (DD fill)	$(2.4\pm0.4) \times 10^{-3}$	100
		Secondary proton ratio (DD fill)	$(1.8\pm0.3) \times 10^{-3}$	78
^{3}He or D$_2$	CD CH	Secondary neutron ratio (D$_2$ fill)	$(3.1\pm0.5) \times 10^{-3}$	94
		D^{3}He proton yield (^{3}He fill)	$(1.3\pm0.2) \times 10^7$	66
		D$_2$ neutron yield (^{3}He fill)	$(8.5\pm0.4) \times 10^8$	97

equally between the clean core and the fuel–shell mix region. The density and temperature profiles of the core and the mix region obtained from this model compare very well with those from 1-D simulations without any mixing, suggesting that the mixing in these implosions does not significantly alter the 1-D, unmixed hydrodynamics of the implosion. This work will be extended to targets with different stability characteristics such as those with thicker shells, lower fill pressures, and different laser pulse shapes. Comparisons of this model with x-ray observables will also be performed in the future.

REFERENCES

1. T. R. Boehly, D. L. Brown, R. S. Craxton, R. L. Keck, J. P. Knauer, J. H. Kelly, T. J. Kessler, S. A. Kumpan, S. J. Loucks, S. A. Letzring, F. J. Marshall, R. L. McCrory, S. F. B. Morse, W. Seka, J. M. Soures, and C. P. Verdon, Opt. Commun. **133**, 495 (1997).

2. P. W. McKenty, V. N. Goncharov, R. P. J. Town, S. Skupsky, R. Betti, and R. L. McCrory, Phys. Plasmas **8**, 2315 (2001).

3. Lord Rayleigh, Proc. London Math Soc. **XIV**, 170 (1883); G. Taylor, Proc. R. Soc. London Ser. A **201**, 192 (1950); R. Betti, V. N. Goncharov, R. L. McCrory, P. Sorotokin, and C. P. Verdon, Phys. Plasmas **3**, 2122 (1996) (and references therein).

4. D. D. Meyerhofer, J. A. Delettrez, R. Epstein, V. Yu. Glebov, V. N. Goncharov, R. L. Keck, R. L. McCrory, P. W. McKenty, F. J. Marshall, P. B. Radha, S. P. Regan, S. Roberts, W. Seka, S. Skupsky, V. A. Smalyuk, C. Sorce, C. Stoeckl, J. M. Soures, R. P. J. Town, B. Yaakobi, J. D. Zuegel, J. Frenje, C. K. Li, R. D. Petrasso, D. G. Hicks, F. H. Séguin, K. Fletcher, S. Padalino, M. R. Freeman, N. Izumi, R. Lerche, T. W. Phillips, and T. C. Sangster, Phys. Plasmas **8**, 2251 (2001); see also Laboratory for Laser Energetics LLE Review **84**, 191, NTIS document No. DOE/SF/19460-371 (2000). Copies may be obtained from the National Technical Information Service, Springfield, VA 22161.

5. Laboratory for Laser Energetics LLE Review **82**, 49, NTIS document No. DOE/SF/19460-344 (2000). Copies may be obtained from the National Technical Information Service, Springfield, VA 22161.

6. E. G. Gamalii *et al.*, JETP Lett. **21**, 70 (1975); T. E. Blue and D. B. Harris, Nucl. Sci. Eng. **77**, 463 (1981); T. E. Blue *et al.*, J. Appl. Phys. **54**, 615 (1983).

7. V. Yu. Glebov, D. D. Meyerhofer, C. Stoeckl, and J. D. Zuegel, Rev. Sci. Instrum. **72**, 824 (2001).

8. F. H. Séguin, C. K. Li, D. G. Hicks, J. A. Frenje, K. M. Green, R. D. Petrasso, J. M. Soures, D. D. Meyerhofer, V. Yu. Glebov, C. Stoeckl, P. B. Radha, S. Roberts, C. Sorce, T. C. Sangster, M. D. Cable, S. Padalino, and K. Fletcher, "Using Secondary Proton Spectra to Study Imploded D_2-Filled Capsules at the OMEGA Laser Facility," submitted to Physics of Plasmas.

9. S. Skupsky and S. Kacenjar, J. Appl. Phys. **52**, 2608 (1981); P. B. Radha, S. Skupsky, R. D. Petrasso, and J. M. Soures, Phys. Plasmas **7**, 1531 (2000).

10. C. K. Li, D. G. Hicks, F. H. Séguin, J. A. Frenje, K. Green, R. D. Petrasso, D. D. Meyerhofer, J. M. Soures, V. Yu. Glebov, P. B. Radha, S. Skupsky, C. Stoeckl, S. Roberts, and T. C. Sangster, "Study of Direct-Drive, DT-Gas-Filled-Plastic-Capsule Implosions Using Nuclear Diagnostics on OMEGA," submitted to Physics of Plasmas.

11. M. C. Richardson, P. W. McKenty, F. J. Marshall, C. P. Verdon, J. M. Soures, R. L. McCrory, O. Barnouin, R. S. Craxton, J. Delettrez, R. L. Hutchison, P. A. Jaanimagi, R. Keck, T. Kessler, H. Kim, S. A. Letzring, D. M. Roback, W. Seka, S. Skupsky, B. Yaakobi, S. M. Lane, and S. Prussin, in *Laser Interaction and Related Plasma Phenomena*, edited by H. Hora and G. H. Miley (Plenum Publishing, New York, 1986), Vol. 7, pp. 421–448.

12. MPI Version 1.2 Standard for IRIX—a communication language for parallel processing (Internet address: http://www.mpi-forum.org) (2001).

13. R. A. Lerche, D. W. Phillion, and G. L. Tietbohl, Rev. Sci. Instrum. **66**, 933 (1995).

14. J. Lindl, Phys. Plasmas **2**, 3933 (1995).